

See discussions, stats, and author profiles for this publication at: <https://www.researchgate.net/publication/361968440>

Mean Reflected Mass: A Physically Interpretable Metric for Safety Assessment and Posture Optimization in Human–Robot Interaction

Conference Paper · May 2022

DOI: 10.1109/ICRA46639.2022.9811582

CITATIONS

2

READS

71

7 authors, including:



Alexander Kurdas

Technische Universität München

10 PUBLICATIONS 33 CITATIONS

[SEE PROFILE](#)



Nico Mansfeld

Franka Emika GmbH

41 PUBLICATIONS 401 CITATIONS

[SEE PROFILE](#)



Mazin Hamad

Chair of Robotics and Systems Intelligence (RSI)

20 PUBLICATIONS 143 CITATIONS

[SEE PROFILE](#)



Robin Jeanne Kirschner

Technische Universität München

21 PUBLICATIONS 109 CITATIONS

[SEE PROFILE](#)

Mean Reflected Mass: A Physically Interpretable Metric for Safety Assessment and Posture Optimization in Human-Robot Interaction

Thomas Steinecker^{1,2}, Alexander Kurdas¹, Nico Mansfeld¹, Mazin Hamad¹, Robin Jeanne Kirschner¹, Saeed Abdolshah¹ and Sami Haddadin¹

Abstract—In physical human-robot interaction (pHRI), safety is a key requirement. As collisions between humans and robots can generally not be avoided, it must be ensured that the human is not harmed. The robot reflected mass, the contact geometry, and the relative velocity between human and robot are the parameters that have the most significant influence on human injury severity during a collision. The reflected mass depends on the robot configuration and can be optimized especially in kinematically redundant robots. In this paper, we propose the Mean Reflected Mass (MRM) metric. The MRM is independent of the direction of contact/motion and enables assessing and optimizing the robot posture w.r.t. safety. In contrast to existing metrics, it is physically interpretable, meaning that it can be related to biomechanical injury data for realistic and model-independent safety analysis. For the Franka Emika Panda, we demonstrate in simulation that an optimization of the robot’s MRM reduces the mean collision force. Finally, the relevance of the MRM for real pHRI applications is confirmed through a collision experiment.

I. INTRODUCTION

To ensure safety in physical human-robot interaction (pHRI) many approaches were introduced, such as safe mechanism design [1], pre-collision schemes [2], or obstacle avoidance [3]. In previous impact studies, we analyzed the role of the reflected mass, i.e., the mass perceived during a collision [4], and the robot velocity on collision safety [5], [6]. In [7] it was then proposed to relate the effective robot mass and the robot velocity to human injury in the event of a collision. This approach provides a maximum allowable robot speed based on the instantaneous reflected mass. During task execution, the robot posture is typically optimized w.r.t. to a certain safety or performance metric. Especially in dexterous collaborative robots, the redundant degrees of freedom can be exploited to perform self-motions that do not affect the primary task. A typical performance metric is the manipulability measure [8], which is often used to avoid singular configurations. In the context of safety, [9] proposed the so-called danger field, whereas [10] proposed to minimize the reflected mass in the direction of motion via self motions. A metric that rates the entire robot posture in terms of safety performance is the Generalized Impact Measure [11], which reflects a measure of sensitivity to impact impulse forces.

¹Technical University of Munich (TUM), Munich Institute of Robotics and Machine Intelligence (MIRMI), Chair of Robotics and System Intelligence (RSI), Munich, Germany, alexander.kurdas@tum.de.

²Institute for Autonomous Systems Technology, Universität der Bundeswehr München, Munich, Germany, thomas.steinecker@unibw.de

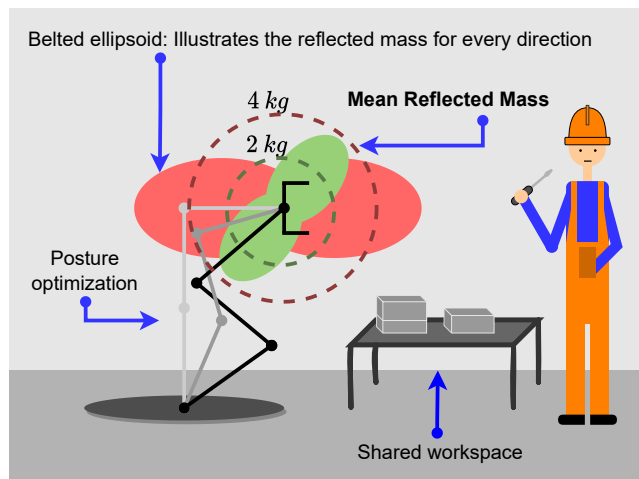


Fig. 1. *Mean Reflected Mass*: A physically interpretable metric for the safety assessment and optimization of the robot’s posture in pHRI. By reconfiguring the robot from the gray to the black configuration, the mean robot reflected mass is reduced, which improves safety in potential collisions with humans and higher velocities can be applied for the end-effector.

In this paper, we introduce the Mean Reflected Mass (MRM) as a novel safety metric. The direction-independent MRM constitutes the average reflected mass over all potential collision directions (see Fig. 1) and is expressed in kilogram and thus physically interpretable. In contrast to other metrics, the MRM can be directly related to human injury data without the need of simplified collision models or intermediate quantities such as force or pressure [7]. We elaborate the MRM in detail and compare the safety performance of our metric and the Generalized Impact Measure (GIM) [11] for a certain workspace range of the Franka Emika Panda in simulation. Furthermore, we conduct impact tests to validate the approach experimentally.

The remainder of this paper is structured as follows. In Sec. II, we describe preliminaries. Sec. III introduces the MRM concept and its mathematical derivation. In Sec. IV, a comparison of MRM and GIM in terms of simulated collision force is provided, and a collision experiment is carried out to evaluate in practice. Finally, Sec. V presents a potential application of the metric for the Safe Motion Unit concept.

II. PRELIMINARIES

Firstly, we summarize the robot dynamics and terminology for modeling the reflected mass. We further introduce the concept of the Safe Motion Unit and explain the well-established metric for dynamic properties, the GIM.

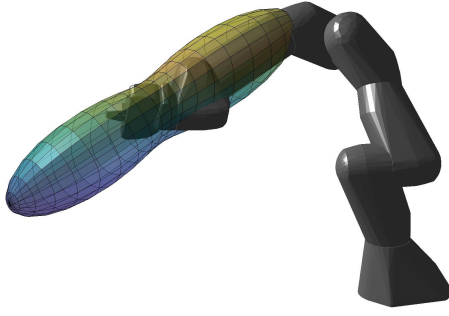


Fig. 2. In this figure, the belted ellipsoid for the Franka Emika Panda is illustrated. It describes the reflected mass in each direction for a given point of a robot, e.g., the end-effector. The belted ellipsoid can be obtained mathematically by squaring the radii of an ellipsoid.

A. Reflected Mass Modeling

The rigid dynamics for a n -joint robot can be expressed as follows

$$\mathbf{M}(\mathbf{q})\ddot{\mathbf{q}} + \mathbf{C}(\mathbf{q}, \dot{\mathbf{q}}) + \mathbf{g}(\mathbf{q}) = \boldsymbol{\tau}, \quad (1)$$

where $\mathbf{q} \in \mathbb{R}^n$ are the generalized coordinates, $\mathbf{M}(\mathbf{q}) \in \mathbb{R}^{n \times n}$ represents the mass matrix, $\mathbf{C}(\mathbf{q}) \in \mathbb{R}^n$ the Coriolis and centrifugal forces, $\mathbf{g}(\mathbf{q}) \in \mathbb{R}^n$ are the forces due to gravity, and $\boldsymbol{\tau} \in \mathbb{R}^n$ are the joint torques. By taking the first derivative of the forward kinematics with respect to time, the following relationship for the Cartesian robot end-effector velocity is obtained

$$\dot{\mathbf{x}} = \mathbf{J}(\mathbf{q})\dot{\mathbf{q}} = \begin{bmatrix} \mathbf{J}_v(\mathbf{q}) \\ \mathbf{J}_w(\mathbf{q}) \end{bmatrix} \dot{\mathbf{q}}, \quad (2)$$

where $\mathbf{J}(\mathbf{q}) \in \mathbb{R}^{6 \times n}$ is the Jacobian matrix. The Jacobian matrices $\mathbf{J}_v(\mathbf{q}) \in \mathbb{R}^{3 \times n}$ and $\mathbf{J}_w(\mathbf{q}) \in \mathbb{R}^{3 \times n}$ represent a linear mapping between the translational velocities and angular velocities in joint space and Cartesian space, respectively. The Cartesian mass matrix (also referred to as Cartesian kinetic energy matrix (KEM)) is given by [4]

$$\boldsymbol{\Lambda}(\mathbf{q}) = (\mathbf{J}(\mathbf{q})\mathbf{M}(\mathbf{q})^{-1}\mathbf{J}(\mathbf{q})^\top)^{-1}. \quad (3)$$

The inverse of this matrix is

$$\boldsymbol{\Lambda}(\mathbf{q})^{-1} = \mathbf{J}(\mathbf{q})\mathbf{M}(\mathbf{q})^{-1}\mathbf{J}(\mathbf{q})^\top = \begin{bmatrix} \boldsymbol{\Lambda}_v(\mathbf{q})^{-1} & \overline{\boldsymbol{\Lambda}}_{v\omega}(\mathbf{q}) \\ \overline{\boldsymbol{\Lambda}}_{v\omega}(\mathbf{q})^\top & \boldsymbol{\Lambda}_\omega(\mathbf{q})^{-1} \end{bmatrix}, \quad (4)$$

where $\boldsymbol{\Lambda}_v(\mathbf{q})^{-1}$, $\boldsymbol{\Lambda}_\omega(\mathbf{q})^{-1}$ and $\overline{\boldsymbol{\Lambda}}_{v\omega}(\mathbf{q})^\top \in \mathbb{R}^{3 \times 3}$ are the translational, rotational and coupling matrices, respectively. Finally, the reflected robot mass is given by

$$m_u(\mathbf{q}) = [\mathbf{u}^\top \boldsymbol{\Lambda}_v(\mathbf{q})^{-1} \mathbf{u}]^{-1}, \quad (5)$$

where $\mathbf{u} \in \mathbb{R}^3$ denotes the evaluation direction. The reflected mass can be represented by a *belted ellipsoid* (see Fig. 2), which is obtained by squaring the distances of an ellipsoid between the center and its surface.

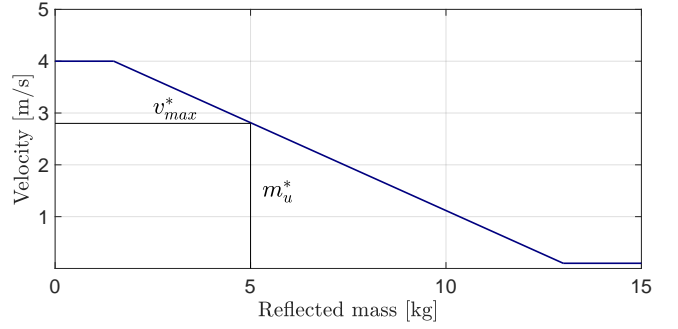


Fig. 3. The figure shows an exemplary safety curve with a spherical impactor of radius 12.5 mm [10]. For a reflected mass m_u^* of 5 kg the robot can move with a velocity v_{max}^* of about 2.8 m/s. As the reflected mass decreases, the robot can proceed faster or be considered safer for the same velocity.

B. Safe Motion Unit

Based on the reflected mass a concept for safe pHRI namely the Safe Motion Unit (SMU) was introduced [7]. The concept is based on a collection of biomechanical injury data [12], which is mapped to the relative human-robot velocity, reflected mass, robot geometry at the location of the potential collision, and the body part of the human at collision. To embed this knowledge into the robot control a threshold for acceptable injuries, i.e., contusion without skin opening, was set. Furthermore, so-called *safety curves* which provide the maximum allowed robot velocity based on the reflected mass were defined, see Fig. 3. Generally, lower reflected mass results in higher safe robot velocity. During task execution, the positions of the human body parts, such as head or hand are tracked and the robot geometry for potential collisions is evaluated. Based on the safety curves for the corresponding human and robot point of interest (POI), safe velocities are identified, and the most conservative of which is considered.

C. Generalized Impact Measure

In [11], a global metric for the dynamic properties of the robot end-effector for specific configuration was introduced, namely the Generalized Impact Measure (GIM). This metric is defined as

$$w_{GIM} = \sqrt{\det((\mathbf{J}_v(\mathbf{q})\mathbf{M}(\mathbf{q})^{-1}\mathbf{J}_v(\mathbf{q})^\top)^{-1})}, \quad (6)$$

which equals the product of the square root of the eigenvalues from the inverse of the KEM. Intuitively speaking, the GIM expresses how difficult it would be for a human to move the end-effector along a translational path in Cartesian space [13]. However, it is devoid of any physical interpretation, made evident by the unit of the metric being $kg^{\frac{3}{2}}$.

III. METHODOLOGY

In this section, we derive the MRM and analyze its properties. First, we elaborate on the meaning and motivation of the MRM. We then establish a relationship between the MRM and the well-known manipulability measure. Finally, the role of this metric in the context of safety concepts based on biomechanical injury data is described.

A. Motivation

Real pHRI, including one or multiple human co-workers, requires the consideration of numerous POIs to ensure safety [7], [10]. By definition, the reflected mass refers to a single POI, as the calculation of the mass requires the knowledge of the direction of the collision and the point of contact. Obtaining this direction in real applications requires reliable sensing of human body parts which adds noise to the calculation, is conceivably not real-time capable, and results in high computational load. Therefore, we aim for a direction-independent metric, which allows optimizing the robot motion velocity by ensuring low injury potential. The GIM (cf. II-C) represents a direction-independent metric, which has been defined, among other applications, for safety-critical applications. However, it lacks physical interpretations by definition. Moreover, it does not consider the reflected mass for calculation, but its square root, consequently this metric is proportional to the volume of the ellipsoid, which is shown in Fig. 4.

Therefore, we introduce a safety-related metric using the average reflected mass in each direction, which reduces the risk of injury equally in each Cartesian direction and is physically meaningful and thus quantitatively assessable. The average reflected mass in each direction expresses the amount of reflected mass that is expected on average over an infinite time horizon and thus it is expressed quantitatively by *kg*.

For safe pHRI applications, the maximum reflected mass appears to play an important role, but we would like to point out that for the concept of the SMU, the severity of a collision is not solely dependent on the mass but on the mass-velocity pair as illustrated in Fig. 3. Thus, safety should be ensured primarily by adhering to the safety curves, while generally providing for a low reflected mass to increase the speed of the robot.

B. Derivation of the Mean Reflected Mass

In the following, the Mean Reflected Mass (MRM) is mathematically derived considering the ellipsoid based on the inverse of the KEM described as

$$\mathbf{u}^T \mathbf{\Lambda}_v(\mathbf{q})^{-1} \mathbf{u} = 1, \quad (7)$$

where $\mathbf{u} \in \{\mathcal{U}\}$ represents the unit direction in \mathbb{R}^3 . The ellipsoid represents the root of the actual reflected mass and can also be expressed as

$$\frac{x^2}{a^2} + \frac{y^2}{b^2} + \frac{z^2}{c^2} = 1. \quad (8)$$

The parameters a , b , and c represent the half-lengths of the major axis of the ellipsoid described in (7) and illustrated in Fig. 4. However, to derive the MRM, an explicit representation of the coordinates is required, which can be specified as

$$\begin{bmatrix} x \\ y \\ z \end{bmatrix} = r \begin{bmatrix} \cos(\gamma) \cos(\lambda) \\ \cos(\gamma) \sin(\lambda) \\ \sin(\gamma) \end{bmatrix}, \quad (9)$$

where

$$r = \frac{abc}{\sqrt{c^2(b^2 \cos(\lambda)^2 + a^2 \sin(\lambda)^2) \cos(\gamma)^2 + a^2 b^2 \sin(\gamma)^2}}. \quad (10)$$

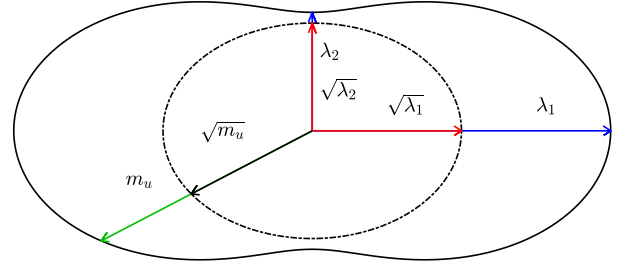


Fig. 4. The figure qualitatively illustrates a belted ellipsoid in planar case. The ellipsoid (ellipse) represents the root of the reflected mass and thus the GIM calculates the product of its eigenvalues. To obtain the actual reflected mass, the length must be squared to obtain the belted ellipsoid (belted ellipse). The direction of the eigenvectors define the orientation of the ellipsoid (ellipse) and the square root of the associated eigenvalue defines the magnitude. The belted ellipsoid is thus completely defined by the eigenvalues and eigenvectors.

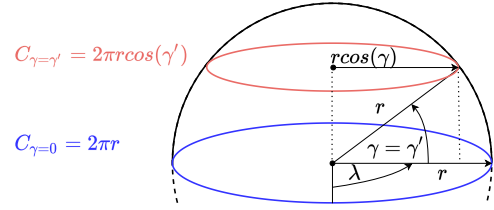


Fig. 5. In the figure the spherical coordinates are shown. It can be seen that with increasing γ , the circumference is scaled with factor $\cos(\gamma)$. Thus the density of the directions decreases by a whole rotation by λ with increasing γ and this must be taken into account for the integration.

It should be noted that γ and λ are the true spherical angles of the ellipsoid. To obtain the actual reflected mass, r has to be squared. An explicit expression has been obtained for which the reflected mass can be calculated depending on the angles γ and λ , given the eigenvalues. In order to calculate the MRM, it is necessary to sum the reflected mass over all directions and then divide by the total number of directions

$$\bar{m}_u = \frac{\sum_{\mathbf{u} \in \{\mathcal{U}\}} m_u(\mathbf{q})}{\text{numel}(\{\mathcal{U}\})}. \quad (11)$$

However, for the integration over all directions the parametrization in (9) must be taken into account. Fig. 5 illustrates the increase of the density of directions with increasing angle γ due to the parametrization. Consequently, we integrate over all radii and divide by the integration over the density of directions, which yields the following result

$$\begin{aligned} \bar{m}_u &= \frac{\int_0^{\pi/2} \int_0^{\pi/2} r^2 \cos(\gamma) d\lambda d\gamma}{\int_0^{\pi/2} \int_0^{\pi/2} \cos(\gamma) d\lambda d\gamma} \\ &= \frac{2 \int_0^{\pi/2} \int_0^{\pi/2} r^2 \cos(\gamma) d\lambda d\gamma}{\pi}. \end{aligned} \quad (12)$$

We make use of the symmetry properties of the belted ellipsoid and consider only one eighth of the entire body for our integration limits.

As (12) cannot be solved analytically, numerical methods are required. Since it involves a double integral, the numerical computational effort is demanding for real-time applications. In this case estimators can provide a suitable solution. Common methods for approximation functions are Gaussian processes or artificial neural networks. For this work, we used artificial neural networks due to their maturity and inherent scalability for large data sets. The training data can be obtained from the numerical computation of (12) and then an estimator of the following form is obtained

$$\bar{m}_u = f_{NN}(a, b, c). \quad (13)$$

We perform a validation test for this estimator (3 layers with 10 neurons each) for a set of 10^5 data points ranging from 0–100 kg with an accuracy of 16 significant digits which results in a root mean square error of $8 \cdot 10^{-4} kg$. The average execution time for 10^6 executions on an *Apple M1* chip was 0.031 ms, which proves the feasibility of the neural network approach. It is noteworthy that this estimator can be used generically for all holonomic robots, since the input variables depend only on the eigenvalues of the KEM and not on specific robot parameters.

C. Relation to Manipulability

In this section, the relation between the MRM and the manipulability is considered. The manipulability was introduced in [8] and can be written as follows

$$\begin{aligned} w_{mani} &= \sqrt{\det \left(\begin{bmatrix} \mathbf{J}_v(\mathbf{q}) \\ \mathbf{J}_w(\mathbf{q}) \end{bmatrix} \begin{bmatrix} \mathbf{J}_v(\mathbf{q})^\top \mathbf{J}_w(\mathbf{q})^\top \end{bmatrix}^\top \right)} \\ &= \sqrt{\det \left(\begin{bmatrix} \mathbf{J}_v(\mathbf{q})\mathbf{J}_v(\mathbf{q})^\top & \mathbf{J}_v(\mathbf{q})\mathbf{J}_w(\mathbf{q})^\top \\ \mathbf{J}_w(\mathbf{q})\mathbf{J}_v(\mathbf{q})^\top & \mathbf{J}_w(\mathbf{q})\mathbf{J}_w(\mathbf{q})^\top \end{bmatrix} \right)}. \end{aligned} \quad (14)$$

From (3) we observe that if the manipulability has a singularity, then so does the inverse of the KEM. However, since only the translational Jacobian is considered, this is also true only for the translational part of the manipulability. A singularity of the KEM correlates with at least one infinitely large eigenvalue, and thus the MRM is also infinitely large. Conversely, it can be shown that optimizing the MRM also avoids singularities of the translational manipulability. An intuitive explanation is that the inverse of the KEM can be interpreted as the weighted manipulability metric where the weighting factor depends on the inertia of the current configuration.

For manipulability, the primary focus is often on avoiding translational and rotational singularities. To account for the rotational manipulability in our MRM optimization, we consider the rotational and coupling part of the manipulability (14) in addition to the MRM

$$\tilde{w}_{mani} = \sqrt{\det(\mathbf{J}_v(\mathbf{q})\mathbf{J}_v(\mathbf{q})^\top - \mathbf{J}_v(\mathbf{q})\mathbf{J}_w(\mathbf{q})^\top)} \rightarrow \max_{\mathbf{q}}. \quad (15)$$

Here, the coupling term $\mathbf{J}_v(\mathbf{q})\mathbf{J}_w(\mathbf{q})^\top$ avoids a linear dependency between the rows of translational and rotational parts of the manipulability measure.

D. Relation to Injury Data

In contrast to many other metrics proposed in robotics literature, the MRM is physically interpretable. This makes the MRM compatible with the data-driven approach proposed in [7], e.g., where the relationship (*mass, velocity, curvature*) \rightarrow *injury* was established. This means that the MRM can be directly related to human injury data and used for the generation of biomechanically safe robot motions.

IV. VALIDATION

In this section, we first investigate the correlation between the MRM and collision force in simulation and then demonstrate the practicality of this metric for pHRI applications using an unconstrained collision test setup.

A. Metrics Comparison

In the following, the correlation between collision force and MRM is investigated and compared to the GIM. The modeled collision force based on a mass-spring system, which was found to be an essential parameter for pHRI applications [5], [14], [15], can be represented as follows for the unconstrained case [14]

$$F_c(m_u) = \sqrt{\frac{m_u M_H}{m_u + M_H}} \sqrt{K_H} v_{re}^0, \quad (16)$$

where M_H is the weight of the human body part, K_H is the contact stiffness and v_{re}^0 is the relative velocity between human and robot. We exemplarily consider a collision with the human head, where $M_H = 4.5$ kg, $K_H = 1000$ N/mm and $v_{re}^0 = 1$ m/s [16].

We calculate the MRM, GIM, and unconstrained collision forces for the Franka Emika Panda robot inside its reference cube given by ISO 9283 [17]. The reference cube has side length 0.4 m and its center is located at $[0.515 \ 0 \ 0.226]^\top$, as provided by the robot's datasheet¹. Furthermore, the orientation is specified for the end-effector along the z_0 -axis.

The evaluation in the cube is performed as follows:

1. All discretized null-space configurations of the robot are determined,
2. for each metric, the smallest value within the reachable null-space configuration is determined,
3. the mean collision forces are calculated for these configurations via (16),
4. the obtained forces are compared to the minimum possible forces over all null-space configurations.

To illustrate the results, all configurations are averaged over the distance to the z_0 -axis, or in other words over the radial distance to the z_0 -axis. The results for this evaluation are depicted in Fig. 6. The results show that the minima of both the MRM and the GIM are similar to the minimum mean collision force over all radial distances.

The reason that the GIM performs worse in approximating the minima is that it calculates the product of the root of the eigenvalues, which takes all directions into account but sets

¹https://wiredworkers.io/wp-content/uploads/2019/12/Panda_FrankaEmika_ENG.pdf

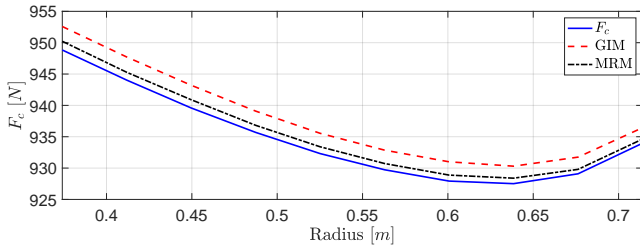


Fig. 6. The figure compares the global minima of the MRM, GIM and mean collision force evaluated as mean collision force. The global minima are determined for each null-space configuration, and the correlating value of the mean collision force is determined. The considered configuration space is defined according to ISO 9283 [17]. The values represent the average over each radius around the z_0 -axis.

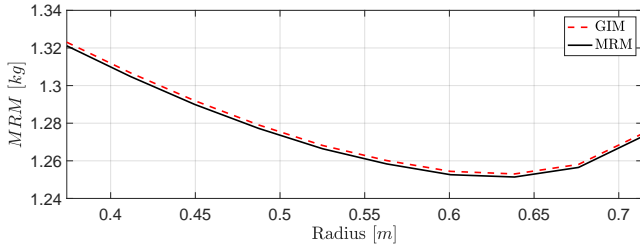


Fig. 7. The figure compares the global minima of the GIM and the MRM evaluated as MRM. The global minima are determined for each null-space configuration, and the correlating value of the MRM for the GIM is determined. The examined configuration space is defined according to ISO 9283 [17]. The values represent the average over each radius around the z_0 -axis.

their weighting purely on the magnitude of the eigenvalues. Thus, a large eigenvalue is weighted proportionally to its magnitude, regardless of how much it contributes over the entire belted ellipsoid. The MRM, on the other hand, considers the overall structure of the belted ellipsoid and evaluates all individual directions. The relation of the collision force as shown in (16) is non-linear and monotonically increasing with respect to the reflected mass. Thus, the progression of the MRM metric which is based on the reflected mass, differs from the mean collision force progression, and a direct scaling between the two is not possible.

In the following, analogous to the minimum collision force comparison, the minimum MRM is plotted over the ISO cube and the MRM value for the minima of the GIM metric depicted in Fig. 7. As expected from the previous observation, the figure shows a similarity between the MRM and the GIM with respect to their minima. However, unlike the GIM, the MRM results provide qualitative statements, e.g., for the Franka Emika Panda, the reflected mass can be optimized to an average of 1.25 kg to 1.32 kg over the entire robot reference cube by a suitable control strategy.

B. Validation of MRM as safety metric

In the following, we validate the MRM as safety-relevant metric. For this, we model two collision scenarios of a Franka Emika Panda robot with an unconstrained mass and use two null-space configurations comprising maximum \mathbf{q}_{\max} and minimum \mathbf{q}_{\min} MRM. We repeat the collisions three

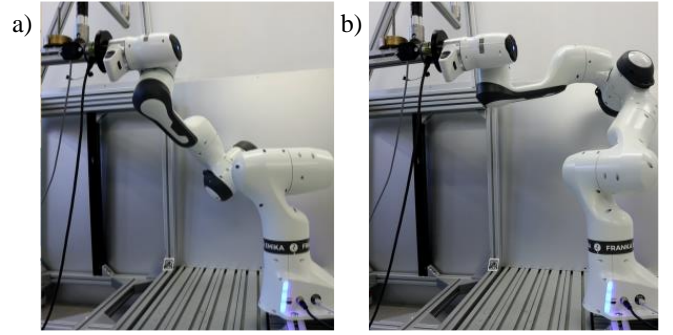


Fig. 8. Experimental setup for validation of the MRM as a safety-relevant metric where a) depicts the collision at \mathbf{q}_{\min} and b) at \mathbf{q}_{\max} .

TABLE I
RESULTS FOR VALIDATION TEST

Scenario	Configuration	Collision force [N]
I	\mathbf{q}_{\min}	121.84 ± 1.72
	\mathbf{q}_{\max}	149.05 ± 6.49
II	\mathbf{q}_{\min}	38.99 ± 0.18
	\mathbf{q}_{\max}	56.17 ± 1.28

times, measure the occurring peak forces, and obtain the average force and standard deviation. We compare whether the results differ significantly to assess the safety-relevance of our proposed metric in collision scenarios.

The experimental setup, depicted in Fig. 8, consists of a pendulum device as described in [18], with 1 kg additional load and a damping cover with 75 ShA. The MRM at the point of collision is 1.38 kg and 2.75 kg for \mathbf{q}_{\min} and \mathbf{q}_{\max} , respectively. A 6-DoF force-torque sensor² is attached to the pendulum collision plate, measuring the occurring collision force at 300 Hz. We apply the joint angles

- a) $\mathbf{q}_{\min} = \{1.81, -1.76, -0.75, -2.43, -2.35, 1.86, -2.27\}$,
- b) $\mathbf{q}_{\max} = \{1.06, -0.98, -0.78, -2.30, -2.08, 2.63, -1.70\}$,

for the robot and collide for the first scenario (I) with a robot velocity of $v_r = 300$ mm/s and in the second scenario (II) $v_r = 150$ mm/s. The resulting collision forces are listed in Tab. I. The resulting difference of $\approx 20\%$ in scenario (I) and $\approx 30\%$ in scenario (II) show a significant, velocity-independent change of the hazard potential when applying our safety metric.

C. Discussion

By comparing the minimum mean collision force and the minimum MRM over the robot's reference cube, we show that the two quantities strongly correlate, implying that optimization with respect to the MRM will strive for configurations that reduce the severity of harm caused by a potential impact as much as possible in all directions. For the MRM, a linear accumulation of all directions is considered. Hence this measure can provide an approximation of the mean collision force without taking into account the external parameters such as weight of the human body part or its stiffness.

²ME-Messsysteme K6D40

Secondly, we show by means of a practical collision test that the minima of the metric correlate with lower forces in the collision and thus the safety of the human can be ensured for higher robot motion velocities which increases the robot performance.

As pointed out in Sec. III-B, no analytical expression for the MRM can be derived, hence the mathematical relationship between the robot configuration and the MRM remains unclear. Although it is possible to evaluate the MRM for a given robot and thus the suitability for pHRI applications as shown in Fig. 6. Due to the lack of an analytical expression, the reverse cannot be done and a suitable robot design strategies cannot be found based on intrinsic MRM insights.

V. MRM IN THE CONTEXT OF THE SAFE MOTION UNIT

In this section, we present the potential of MRM for the Safe Motion Unit (SMU). The SMU is based on biomechanical injury data and represents a relationship between the reflected mass and the maximum allowable robot velocity. The reflected mass is a quantity that depends on both the configuration and a Cartesian direction, which is usually the measured position of the human. However, in pHRI applications, it is possible that the most endangered body part (from the controller's point of view) changes abruptly, e.g., from the hand to the head. In addition, the measurement noise and perceptual inaccuracy may not be reliable enough for pHRI applications.

This is where the MRM can provide a remedy due to its independence from external parameters and its link to biomechanical injury data. The MRM represents an average value in mass that can be expected in a collision, and through this interpretation it can directly make a statement based on biomechanical injury data. The SMU is a control concept that adjusts velocity based on injury-related parameters. By coupling with the MRM for optimization, mass can be reduced in all directions and control can be decoupled from velocity adjustment. As shown in Sec. III-B, the MRM can be computed in real-time, thus making this approach plausible.

In the following, we propose a more sophisticated control concept analogous to the reflected mass control in [10] that attempts to achieve the global minima of the MRM:

1. Analyze the entire self-motion manifolds of a robot, as shown in [19], [20].
2. A discretized set of all relevant robot configurations over all null-space configurations for which the MRM is minimal are calculated offline. These configurations are then stored in a database.
3. Throughout control, the configurations from the database are utilized as attractive minima for redundancy resolution optimization.

With this control approach, the global minima are approximated, and thus MRM values can be achieved for the configurations as defined in ISO 9283 [17] for the Franka Emika Panda, as described in Fig. 7.

VI. CONCLUSION

In this paper, we proposed the Mean Reflected Mass (MRM), a metric for safety assessment and posture optimization in physical human-robot interaction (pHRI). We investigated the performance of the MRM in simulation for a typical workspace area of the Franka Emika Panda robot and validated the metric in collision experiments. In comparison to existing safety metrics, the MRM has a real physical interpretation, it is the configuration-dependent average reflected mass in all directions. The MRM can be directly related to human injury data, which makes it a powerful and meaningful metric for robot motion control.

ACKNOWLEDGEMENTS

This work was supported by the European Union's Horizon 2020 research and innovation programme as part of the projects DARKO (grant no. 101017274), and I.A.M. (grant no. 871899). Furthermore, we gratefully acknowledge the support of the Lighthouse Initiative KI.FABRIK Bayern by StMWi Bayern (KI.FABRIK Bayern Phase 1: Aufbau Infrastruktur und KI.Fabrik Bayern Forschungs- und Entwicklungsprojekt, grant no. DIK0249), the Lighthouse Initiative Geriatrics by StMWi Bayern (Project X, grant no. IUK-1807-0007// IUK582/001), and the LongLeif GaPa gGmbH (Project Y). The authors would like to thank the Bavarian State Ministry for Economic Affairs, Regional Development and Energy (StMWi) for financial support as part of the project SafeRoBAY (grant no. DIK0203/01). Please note that S. Haddadin has a potential conflict of interest as shareholder of Franka Emika GmbH.

REFERENCES

- [1] K. Ikuta, H. Ishii, and M. Nokata, "Safety evaluation method of design and control for human-care robots," *The International Journal of Robotics Research*, vol. 22, no. 5, pp. 281–297, 2003.
- [2] D. Kulić and E. Croft, "Pre-collision safety strategies for human-robot interaction," *Autonomous Robots*, vol. 22, no. 2, pp. 149–164, 2007.
- [3] F. Flacco, T. Kröger, A. De Luca, and O. Khatib, "A depth space approach to human-robot collision avoidance," in *2012 IEEE International Conference on Robotics and Automation*. IEEE, 2012, pp. 338–345.
- [4] O. Khatib, "Inertial properties in robotic manipulation: An object-level framework," *The international journal of robotics research*, vol. 14, no. 1, pp. 19–36, 1995.
- [5] S. Haddadin, A. Albu-Schäffer, and G. Hirzinger, "Requirements for safe robots: Measurements, analysis and new insights," *The International Journal of Robotics Research*, vol. 28, no. 11-12, pp. 1507–1527, 2009.
- [6] R. J. Kirschner, N. Mansfeld, G. G. Peña, S. Abdolshah, and S. Haddadin, "Notion on the correct use of the robot effective mass in the safety context and comments on ISO/TS 15066," in *2021 IEEE International Conference on Intelligence and Safety for Robotics (ISR)*. IEEE, 2021, pp. 6–9.
- [7] S. Haddadin, S. Haddadin, A. Khoury, T. Rokahr, S. Parusel, R. Burgkart, A. Bicchi, and A. Albu-Schäffer, "On making robots understand safety: Embedding injury knowledge into control," *The International Journal of Robotics Research*, vol. 31, no. 13, pp. 1578–1602, 2012.
- [8] T. Yoshikawa, "Manipulability of robotic mechanisms," *The international journal of Robotics Research*, vol. 4, no. 2, pp. 3–9, 1985.
- [9] B. Lacevic, P. Rocco, and A. M. Zanchettin, "Safety assessment and control of robotic manipulators using danger field," *IEEE Transactions on Robotics*, vol. 29, no. 5, pp. 1257–1270, 2013.

- [10] N. Mansfeld, B. Djellab, J. R. Veuthey, F. Beck, C. Ott, and S. Haddadin, "Improving the performance of biomechanically safe velocity control for redundant robots through reflected mass minimization," in *2017 IEEE/RSJ International Conference on Intelligent Robots and Systems (IROS)*. IEEE, 2017, pp. 5390–5397.
- [11] I. D. Walker, "Impact configurations and measures for kinematically redundant and multiple armed robot systems," *IEEE transactions on robotics and automation*, vol. 10, no. 5, pp. 670–683, 1994.
- [12] N. Mansfeld, M. Hamad, M. Becker, A. G. Marin, and S. Haddadin, "Safety map: A unified representation for biomechanics impact data and robot instantaneous dynamic properties," *IEEE Robotics and Automation Letters*, vol. 3, no. 3, pp. 1880–1887, 2018.
- [13] T. Yoshikawa, "Dynamic manipulability of robot manipulators," *Transactions of the Society of Instrument and Control Engineers*, vol. 21, no. 9, pp. 970–975, 1985.
- [14] ISO/TS 15066, "Robots and robotic devices – Collaborative robots," International Organization for Standardization, Geneva, CH, Technical Specification, Feb. 2016.
- [15] K. Suita, Y. Yamada, N. Tsuchida, K. Imai, H. Ikeda, and N. Sugimoto, "A failure-to-safety "kyozon" system with simple contact detection and stop capabilities for safe human-autonomous robot coexistence," in *Proceedings of 1995 IEEE International Conference on Robotics and Automation*, vol. 3. IEEE, 1995, pp. 3089–3096.
- [16] B. Siciliano, O. Khatib, and T. Kröger, *Springer handbook of robotics*. Springer, 2008.
- [17] ISO 9283:1998-04, "Manipulating industrial robots – Performance criteria and related test methods," International Organization for Standardization, Geneva, CH, Standard, Apr. 1998.
- [18] R. J. Kirschner, J. Jantalia, N. Mansfeld, S. Abdolshah, and S. Haddadin, "CSM: Contact sensitivity maps for benchmarking robot collision handling systems," in *2021 International Conference on Robotics and Automation (ICRA)*, 2021.
- [19] J. W. Burdick, "On the inverse kinematics of redundant manipulators: Characterization of the self-motion manifolds," in *Advanced Robotics: 1989*. Springer, 1989, pp. 25–34.
- [20] C. L. Luck and S. Lee, "Redundant manipulator self-motion topology under joint limits with an 8-dof case study," in *Proceedings of 1993 IEEE/RSJ International Conference on Intelligent Robots and Systems (IROS'93)*, vol. 2. IEEE, 1993, pp. 848–855.